# Coupled redox transformations of catechol and cerium at the surface of a cerium(III) phosphate mineral

Javiera Cervini-Silva [a,b,*], Benjamin Gilbert [c], Sirine Fakra [c], Stephan Friedlich [d], Jillian Banfield [b,c,e]

[a] *Universidad Nacional Autónoma de México, Instituto de Geografía, Circuito Exterior, Ciudad Universitaria, Coyoacan, C.P. 04150, México City, Mexico*
[b] *NASA Astrobiology Institute, University of California Berkeley, Berkeley, CA 94720-3110, USA*
[c] *Lawrence Berkeley National Laboratory, 1 Cyclotron Road, Berkeley, CA 94720, USA*
[d] *Lawrence Livermore National Laboratory, 7000 East Avenue, Livermore, CA 94550, USA*
[e] *Department of Earth and Planetary Science, University of California Berkeley, 307 McCone Hall, Berkeley, CA 94720-4767, USA*

**Abstract**

Highly insoluble Ce-bearing phosphate minerals form by weathering of apatite [$Ca_5(PO_4)_3.(OH,F,Cl)$], and are important phosphorous repositories in soils. Although these phases can be dissolved via biologically-mediated pathways, the dissolution mechanisms are poorly understood. In this paper we report spectroscopic evidence to support coupling of redox transformations of organic carbon and cerium during the reaction of rhabdophane ($CePO_4{\cdot}H_2O$) and catechol, a ubiquitous biogenic compound, at pH 5. Results show that the oxic–anoxic conditions influence the mineral dissolution behavior. Under anoxic conditions, the release of P and Ce occurs stoichiometrically. In contrast, under oxic conditions, the mineral dissolution behavior is incongruent, with dissolving $Ce^{3+}$ ions oxidizing to $CeO_2$. Reaction product analysis shows the formation of $CO_2$, polymeric C, and oxalate and malate. The presence of more complex forms of organic carbon was also confirmed. Near edge X-ray absorption fine structure spectroscopy measurements at Ce-$M_{4,5}$ and C-K absorption edges on reacted $CePO_4{\cdot}H_2O$ samples in the absence or presence of catechol and dissolved oxygen confirm that (1) the mineral surface converts to the oxide during this reaction, while full oxidation is limited to the near-surface region only; (2) the Ce valence remains unchanged when the reaction between $CePO_4{\cdot}H_2O$ and $O_2$ but in the absence of catechol. Carbon K-edge spectra acquired from rhabdophane reacted with catechol under oxic conditions show spectral features before and after reaction that are considerably different from catechol, indicating the formation of more complex organic molecules. Decreases in intensity of characteristic catechol peaks are accompanied by the appearance of new $\pi^*$ resonances due to carbon in carboxyl (ca. 288.5 eV) and carbonyl (ca. 289.3 eV) groups, and the development of broad structure in the $\sigma^*$ region characteristic of aliphatic carbon. Evolution of the C K-edge spectra is consistent with aromatic-ring cleavage and polymerization. These results further substantiate that the presence of catechol, $O_2$ (aq) causes both the oxidation of structural $Ce^{3+}$ and the transformation of catechol to more complex organic molecules. Scanning Transmission X-Ray Microscopy measurements at the C K and Ce $M_{4,5}$ edges indicate three dominant organic species, varying in complexity and association with the inorganic phase. Untransformed catechol is loosely associated with $CeO_2$, whereas more complex organic molecules that exhibit lower aromaticity and stronger C=O $\pi^*$ resonances of carboxyl-C and carbonyl-C groups are only found in association with the grains. These results further serve as basis to postulate that, in the presence of $O_2$, $CeO_2$ can mediate the oxidative polymerization of catechol to form higher molecular weight polymers. The present work provides evidence for a pathway of biologically-induced, non-enzymatic oxidation of cerium and formation of small $CeO_2$ particles at room temperature. These findings may have implications for carbon cycling in natural and cerium-contaminated soils and aqueous environments.


* Corresponding author. Fax: +52 55 5616 2145.
*E-mail address:* jcervini@igg.unam.mx (J. Cervini-Silva).

## 1. INTRODUCTION

Phosphate bioavailability can limit ecosystem productivity. In near-surface low-temperature geological settings, phosphorus is generally partitioned between the aqueous phase, organic matter, mineral surfaces, primary phosphate phases (such as apatite) and secondary phosphates (commonly trivalent metal phosphate minerals) (Banfield and Eggleton, 1989). For microbial productivity, phosphate limitation may occur due to sequestration of phosphate into insoluble secondary phosphate minerals or through incorporation of phosphate into recalcitrant organic complexes, such as phosphohumate complexes (Crews et al., 1995). The formation of secondary phosphate phases is a function of the localized availability of phosphate and lanthanide ions. For example, microcrystalline lanthanide-bearing phosphate minerals may form as a result of apatite [$Ca_5(PO_4)_3(OH,Cl,F)$] and allanite [$Ce_2(Al)_3(SiO)_4OH$] weathering.

Microcrystalline lanthanide-bearing phosphate minerals are important metal and phosphorous repositories in soils and other subsurface environments (Banfield and Eggleton, 1989). However, in soils where secondary phosphate minerals, including lanthanide phosphates, are the dominant source of phosphorous, the colonization of mineral surfaces by native microbial communities can lead to their dissolution (Taunton et al., 2000a,b). Although lanthanide phosphate minerals are highly insoluble (solubility product $= 10^{-24} - 10^{-26}$; Jonasson et al., 1985), colonization of their surfaces by native microbial communities can lead to mineral dissolution (Taunton et al., 2000a,b). This has been attributed to the combined effects of the complexation of aqueous lanthanide ions by organic ligands and microbial phosphorus uptake (Taunton et al., 2000a). In some cases, dissolution of lanthanide phosphate minerals in oxidized soils is accompanied by the precipitation of nanocrystalline $CeO_2$ (Green et al., 2002).

Cerium is the most abundant lanthanide and generally the only one to undergo redox reactions at the Earth's surface. In young weathering profiles, field data suggest that most Ce exists as $Ce^{3+}$, whereas in older weathered profiles $Ce^{3+}$ is oxidized to $Ce^{4+}$ (Taunton et al., 2000a,b). It has been shown previously that dissolution of phosphate minerals containing $Ce^{3+}$ is accompanied by cerium oxidation and precipitation of nanocrystalline $CeO_2$ (Gardner et al., 1983; Jonasson et al., 1985; Banfield et al., 1999; Taunton et al., 2000a,b; Cervini-Silva et al., 2005). These processes are believed to be responsible for the accumulation of Ce at the top of the saprolite layers of lateritic soil profiles (Braun et al., 1990) and the depletion of dissolved Ce in the oceans relative to other lanthanides (Moffett, 1990, 1993). Oxidation of $Ce^{3+}$ by $O_2$ in seawater is extremely slow, but is accelerated by microorganisms (Moffett, 1990, 1993), and it has been proposed that $Ce^{3+}$ oxidation occurs enzymatically (Moffett, 1990, 1993).

Although redox reactions involving Ce-rich phosphate minerals may affect the stability of lanthanide phosphate minerals in soil and marine environments, little attention has been paid to the role of biogenic molecules (other than enzymes) in $Ce^{3+}$ redox transformations, or to the possible implications of such reactions for carbon cycling. Organic compounds secreted into the subsurface environment by microbes and plants can interact with surface-bound phosphate, increasing availability of phosphorus for plant uptake (Barber and Martin, 1976; Brewster et al., 1976; Nye, 1977; Kucey et al., 1989). For example, low-molecular weight organic acids can readily induce the release of phosphate through the dissolution of apatite (Welch et al., 2002). Other organics such as polysaccharides may promote mineral dissolution by complexing with ions in solution, thereby lowering the minerals' solution saturation state (Welch and Vandevivere, 1994; Banfield et al., 1999; Welch et al., 1999). In addition, biogenic compounds such as citrate, secreted by some plants, may form polymers with iron and phosphate, which can effectively increase their concentration in the soil solution in proximity to the plant's roots (Gardner et al., 1983). For example, the secretion of citrate by *Lupinus albus* L. ($\leqslant$188 mg citrate per total weight (g) of soil at pH 5) causes the proximal dissolution of phosphate ferric hydroxides and the concomitant release of iron and phosphate. Dissolved Fe and citrate then form polymers such as $[(FeO)_{0.95}(OH)_{0.75}(citrate)_{0.15}Na_{0.24}]_n$ (Gardner et al., 1983).

Abiotic experimentation provides evidence for the significance of biogenic compounds in mineral dissolution. For instance, small organics such as malate (Jauregui and Reisenauer, 1982), glutamate (Traina and Doner, 1985), diphenolics, salicylic acid, pyruvic acid, oxalic acid, fulvic acid (Stone and Morgan, 1984, 1987), or even monophenolic compounds sharing electron donating substituents (Lehmann et al., 1987; Stone, 1987; McBride, 1989a,b) facilitate the reductive dissolution of Mn oxides and become oxidized as a result. Because $Ce^{4+}$ is a stronger oxidant than manganese (Larson and Hufnal, 1980; Machjer et al., 2000), it is likely to participate in similar geochemical cycles to $Mn^{4+}$.

We investigate here the redox mineral transformations during the reaction of $CePO_4{\cdot}H_2O$ with catechol ($C_6H_6O_2$). Catechol is a ubiquitous biogenic compound known to undergo mineral-mediated electron transfer processes (Larson and Hufnal, 1980; Bennett, 1991; Welch and Ullman, 1992; Wang and van Capellen, 1996; Larson, 1998; Kinrade et al., 1999; Machjer et al., 2000; Sparks, 2003). Catechol is also typical intermediate in aerobic hydrocarbon degradation and has been shown to accelerate the weathering of primary silicates via the formation of stable complexes with Si and Al (Bennett, 1991; Welch and Ullman, 1992; Wang and van Capellen, 1996; Kinrade et al., 1999). We show that catechol induces oxidation of $Ce^{3+}$ to form $CeO_2$ and is degraded by $CeO_2$ production at room temperature. The outcome of this work contributes to a better understanding of the effect of biological activity on the stability of secondary phosphate minerals and their transformation is relevant to predictions of the stability of lanthanide phosphate compounds. In this paper, we aim to study rare-earth orthophosphates such as rhabdophane ($CePO_4{\cdot}H_2O$) are amongst the most insoluble materials (solubility product $K_{sp} = 10^{-25}$; Firsching and Brune, 1991). Due to their low solubility, they are used as chemical tracers of natural fluid–rock processes (Ushakov et al., 2001), have been studied extensively for *c* long-term storage

of nuclear wastes, and are under consideration as host phases for actinides.

## 2. MATERIALS AND METHODS

*Materials*. Catechol (99% powder; CAS Number: 120-80-9), oxalic acid (99% ⩽; CAS Number: 144-62-7), Malic acid (CAS Number: 6915-15-7), humic acid (CAS Number: 1415-93-6), and cerium oxide (CAS Number: 1306-38-3) were purchased from Sigma–Aldrich. Natural humic samples were kindly arranged by Prof. Garrison Sposito (University of California) and referred thereafter as compounds 1, 2, and 3 (peroxidase extracted humic acid), 4 (4,5-dichlorocatechol), 5 (2,3,4-trihydroxybenzoic acid), and 6 (Greenfield humic acid).

### 2.1. Mineral characterization

Cerium phosphate was synthesized by rapidly mixing 0.5 M phosphoric acid and cerium chloride solutions at 20 °C, as described elsewhere (Hikichi et al., 1978). Solid samples were separated from the liquor and rinsed with distilled water until the pH of the supernatant solution was $5.7 \pm 0.2$. pH measurements were conducted before conducting dissolution experiments.

Powder X-ray diffraction (XRD) analysis confirmed the solid to be a mixture of rhabdophane and monazite, polymorph phases of $CePO_4$. The specific surface areas for $CePO_4{\cdot}H_2O$ samples and commercial $CeO_2$ were $66 \pm 1$ and $19.7 \pm 1\ m^2\ g^{-1}$, as described by the static BET method.

### 2.2. Mineral dissolution

Dissolution of $CePO_4{\cdot}H_2O$ was investigated in batch mode in filter-sterilized (0.2 μm filter) 1 mM catechol at pH 5.0, solids concentration of $1\ g\ L^{-1}$, constant stirring, under oxic and anoxic conditions for periods of 7 days. Dissolution experiments under strict anoxic conditions were prepared inside a Coy environmental chamber (Grass Lake, MI) equipped with a gas analyzer and a catalytic regenerator. Anoxic stock solutions were prepared by degassing distilled water with high purity nitrogen gas ($15\ min\ L^{-1}$ water). The samples were then handled in a glove box. The content of dissolved oxygen during the experiments was monitored using an oxygen meter (Unisense, Denmark). Dissolved oxygen contents measured in oxic and anoxic solutions corresponded to $8.1 \pm 0.1$ and $\leqslant 0.01\ mg\ L^{-1}$, respectively. All batch experiments conducted under anoxic conditions were septum sealed and covered with parafilm, and opened prior analysis inside the environmental chamber.

Aliquots of HCl or NaOH were added for pH adjustment. Variations in pH in suspensions bearing $CePO_4{\cdot}H_2O$ and catechol were kept at <0.1 pH units. After equilibration, the suspensions were centrifuged and the supernatant solutions filtered for chemical analysis using 0.02 μM-Millipore syringe filters. Ce and P determinations were conducted using an inductively-coupled plasma atomic emission spectrometer (ICP-AES), with emission lines at 418.6 and 178.7 nm, respectively.

Two-hundred hour adsorption experiments were also conducted and the supernatant solutions filtered for catechol determination. Catechol ligand disappearance was quantified using a UV spectrometer at $\lambda = 275$ nm (Larson and Hufnal, 1980). Catechol solutions used in experiments and inorganic oxidation controls were monitored spectroscopically.

Additional experiments were conducted to study whether the formation of $CeO_2$ could occur in the absence of $CePO_4{\cdot}H_2O$ as $Ce^{3+}$ source. The initial reaction conditions were (a) $5 \times 10^{-6}$ M $CeCl_3$ and $9.9 \times 10^{-4}$ M catechol, (b) $4 \times 10^{-5}$ M $CeCl_3$ and $9.1 \times 10^{-4}$ M catechol, and (c) $1.1 \times 10^{-4}$ M $CeCl_3$ and $1 \times 10^{-3}$ M catechol. Determinations of $[Ce^{3+}]$ (as total, dissolved Ce) and dissolved oxygen were conducted as described above by ICP-AES and oxygen meter, respectively. In addition, equivalent experiments investigated the ability of pure $CeO_2$ to catalyze the oxidation of catechol in the presence of $O_2$.

### 2.3. Reaction products analysis

#### *2.3.1. Bulk solution and head space*

Identification and quantification of reaction products in supernatant solutions was conducted using a Shimadzu SPD high pressure liquid chromatograph equipped with a UV detector and a Hamilton HC-75 column (protonated form). A 20-min program was used with a flow rate of $0.4\ mL\ min^{-1}$ and a mobile phase of 0.016 N $H_2SO_4$ in distilled water. Elution times for oxalate, malate, and catechol were 2–3.1, 6.1–7.0, and 8.5–9.5 min, respectively.

Total organic and inorganic carbon analysis of supernatant solutions was conducted using a 1010 O-I-Analytical total organic carbon analyzer equipped with a 1051 vial multisampler (College Station, TX). Evolution of $CO_2$ was determined by head-space sampling and analyzed using a gas chromatograph equipped with a total carbon detector 8610 SRI (Torrace, CA), and corrected for $CO_2$ atmospheric levels at 25°C. Suspensions were not purged for $CO_2$ trapping. An gas-tight syringe was used for headspace sampling at various time intervals. Experiments were reproduced such that vials were used for analyses only once. Experiments were conducted in 3-mL gas-tight vials.

Pentane-extractions of mineral samples in aqueous solution were conducted to recover the sorbed, non-polymeric catechol. Polymeric catechol was estimated from determinations of the carbon content in mineral samples as determined by thermogravimetry.

Reported percentage weight for the conversion of C (% wt C) in suspension are referred to initial concentrations of catechol in solution.

#### *2.3.2. Powder X-ray diffraction*

XRD analysis of the initial and transformed $CePO_4{\cdot}H_2O$ material was performed by drying the wet powder on a low background quartz plate for measurement with a X'Pert Pro X-ray Diffractometer (Panalytical), using Co K(α) radiation (1.7903 Å).

*2.3.3. X-ray spectroscopy and spectromicroscopy*

Near edge X-ray absorption fine structure (NEXAFS) spectroscopy measurements at Ce $M_{4,5}$ and C K absorption edges on weathered $CePO_4{\cdot}H_2O$ samples in the absence or presence of catechol and dissolved oxygen were conducted on beamline 4.0.2 at the Advanced Light Source, Lawrence Berkeley National Laboratory (Young et al., 2001). The spectroscopic data were obtained by scanning the X-ray energy through the Ce $M_{4,5}$ edges with an approximate energy resolution of 0.2 eV and measuring the absorption signal through the total electron yield (TEY) with a channeltron electron-multiplier. The raw TEY signal was normalized by the incident beam intensity ($I_0$), a smooth polynomial background and an arctangent step jump function were fitted to the data and the absorption step was set to unity.

Scanning transmission X-ray microscopy (STXM) measurements at the C K and Ce $M_{4,5}$ edges were conducted at the Molecular Environmental Science beamline 11.0.2 of the Advanced Light Source at Lawrence Berkeley National Laboratory (Tyliszczak et al., 2004). The STXM uses a Fresnel zone plate lens to focus a monochromatic soft X-ray beam onto a sample that is $X$–$Y$ raster scanned. Transmitted photons were detected via a phosphor scintillator photomultiplier tube assembly, linear up to 15 MHz. This technique, pioneered by Kirz et al. (1995), is based on core electron excitation by X-ray absorption, which provides the imaging contrast. Transmission images at energies below and at the relevant absorption edges and subsequently converted into optical density images were used to derive chemical maps. Image sequences (called stacks) acquired at multiple energies spanning the relevant element absorption edge were used to extract NEXAFS spectra from areas of interest on the samples. The theoretical spectral resolution during our measurements was 100 meV and the energy was calibrated at the C K-edge using the 3p Rydberg peak of gaseous $CO_2$ at 294.96 eV, and at the Ce $M_{4,5}$-edges using the Ce $M_5$-edge of $CePO_4{\cdot}H_2O$ at 882.8 eV.

To check for radiation induced damage on our organic samples, we collected fast stacks, using fewer spectral and spatial points and fast dwell times (0.2 ms) using small slit sizes in regions similar to the ones of interest and compared them with finer stacks performed on regions of interest. No alteration of the spectra was observed under careful conditions (incident flux $<10^7$ photons/s, fast dwell times $<0.5$ ms). The images in each sequence were aligned via a spatial cross-correlation analysis using the aXis2000 software. Absorption spectra were extracted from groups of pixels from relevant spatial areas of the stack. Clean areas of the silicon nitride membrane were used to normalize the absorption signal obtained from the areas of interest.

One microliter of cerium weathered solutions was deposited using a micropipette onto a $Si_3N_4$ window (Silson Ltd.), 100 nm thick, then air-dried. All reference compounds were in powder form and finely ground using an agate mortar and pestle. They were then suspended in MQ water, deposited onto a $Si_3N_4$ membrane using a micropipette and air-dried. All samples were analyzed under He near atmospheric pressure.

## 3. RESULTS AND DISCUSSION

### 3.1. Cerium redox transformation

Fig. 1 shows the solubilization of Ce and phosphate during the batch dissolution of microcrystalline $CePO_4{\cdot}H_2O$ in the presence of 1 mM catechol under oxic and anoxic conditions at pH 5. Concentrations of [Ce] and [P] following mineral dissolution in the presence of water only at $pH_0 = 5$ were found to be below detection limits. When $CePO_4{\cdot}H_2O$ was dissolved in the absence of $O_2$, Ce ions accumulated in solution (ca. $20 \times 10^{-6}$ M). However, when dissolution occurred in the presence of $O_2$, Ce concentration in solution did not surpass $6 \times 10^{-6}$ M, indicating the formation of a Ce-sequestering solid product. Our results show that Ce:P molar ratios in solution after reacting $CePO_4{\cdot}H_2O$ under anoxic and oxic conditions were found to be ca. 1:1 and $10\leqslant$, respectively. In contrast, concentrations of Ce were found to be up to four times or higher for the case when experiments were conducted under anoxic conditions.

Experiments were conducted to study whether Ce oxidation could occur using another Ce(III) source. The fate of aqueous Ce(III) (as $CeCl_3$) in the presence of $O_2$ and catechol at room temperature and pH 5 was studied. Decreases in Ce(III) concentration in solution, [Ce(III)], were determined using a UV spectrometer. Results depicted in Fig. 2 show that the reaction between aqueous Ce(III)

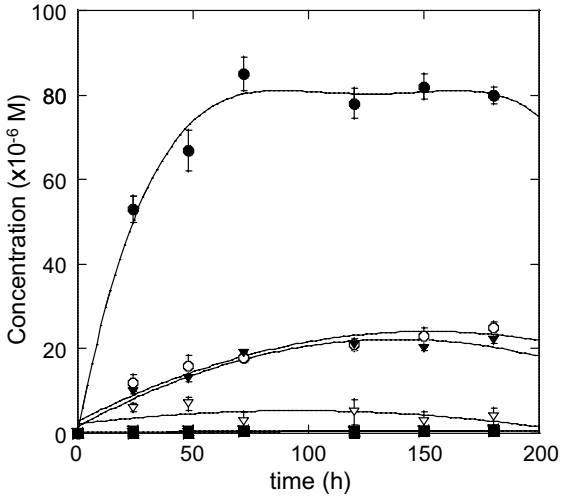


Fig. 1. The accumulation of cerium and phosphorous during the reaction of catechol with $CePO_4{\cdot}H_2O$ at pH 5. The accumulation of cerium and phosphorous after reaction with catechol under oxic conditions is represented by open triangles and solid circles, respectively. The accumulation of cerium and phosphorous after reaction with catechol under anoxic conditions is represented by solid triangles and open circles, correspondingly. Solid squares represent the accumulation of cerium and phosphorous during the dissolution of $CePO_4{\cdot}H_2O$ at pH 5 under oxic conditions in the absence of catechol. The concentrations of solid and catechol were 1 g $L^{-1}$ and $1 \times 10^{-3}$ M, respectively. The initial dissolved oxygen concentrations for the cases referred to as oxic and anoxic conditions corresponded to $8.1 \pm 0.1$ and $\leqslant 0.01$ mg $L^{-1}$, respectively.

and $O_2$ using $CeCl_3$ as the Ce(III) source is very slow, except in the presence of catechol. The oxidation of Ce(III) is fastest when the concentration of aqueous cerium is low ($[Ce]_0$ ca. $5 \times 10^{-6}$ or $4 \times 10^{-5}$ M) and the Ce(III)-to-catechol molar ratio is <0.05. Under these conditions, the complexation by catechol appears to mediate the oxidation of Ce(III) ions. Once formed, Ce(IV) can react with catechol to form low-molecular weight organic compounds (see below).

Cerium oxidation is inhibited at higher initial concentrations of aqueous cerium ($1.1 \times 10^{-4}$ M) and catechol ($10^{-3}$ M) under oxic conditions, possibly due to the formation of $Ce^{4+}$-catechol complexes such as $[Ce(cat)_4]^{4-}$. Such complexes owe their existence and stability to the coordination ability of catechol (Sofen et al., 1979). It is possible that similar pathways prevail in concentrated suspensions of $CePO_4{\cdot}H_2O$ and catechol that could preclude the formation of Ce(IV)-bearing clusters (Sofen et al., 1979).

### 3.2. Solid product analysis

#### *3.2.1. The formation of $CeO_2$*

Two conventional analysis methods indicated that $CeO_2$ is the mineral product of the oxidation of $CePO_4{\cdot}H_2O$ in the presence of catechol. Powder X-ray diffraction patterns of synthetic $CePO_4{\cdot}H_2O$ dissolved in catechol under oxidizing conditions for several weeks showed a characteristic peak that can be assigned to the (111) reflection of $CeO_2$ (Fig. 3). However, the extent of transformation was small, and a full $CeO_2$ pattern could not be resolved. Prior work report infrared spectra of reacted $CePO_4{\cdot}H_2O$ samples indicate the presence of a doublet at 2360 $cm^{-1}$, characteristic of $CeO_2$ (Cervini-Silva et al., 2005). The oxidation of structural Ce was further confirmed by Ce NEXAFS Spectroscopy.

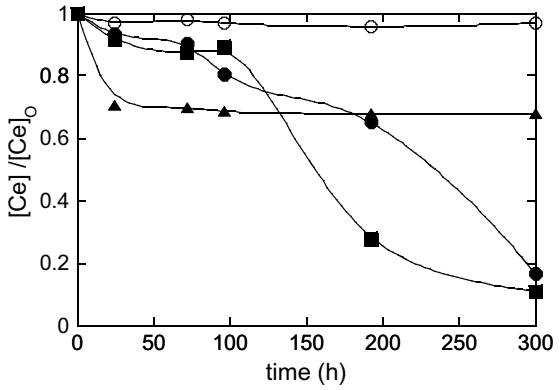


Fig. 2. Time dependence of the oxidation of aqueous $Ce^{3+}$, as a fraction of the total, dissolved Ce for various reaction conditions: $5 \times 10^{-6}$ M $CeCl_3$ and $9.9 \times 10^{-4}$ M catechol (solid circles); $4 \times 10^{-5}$ M $CeCl_3$ and $9.1 \times 10^{-4}$ M catechol (squares); and $1.1 \times 10^{-4}$ M $CeCl_3$ and $1 \times 10^{-3}$ M catechol (triangles) at pH 5. Open circles represent control experiments of $Ce^{3+}$ concentration at pH 5 in the absence of catechol. The initial dissolved oxygen concentrations corresponded to $8.1 \pm 0.1$ mg $L^{-1}$.

#### *3.2.2. Ce and C NEXAFS spectroscopy: dissolved oxygen mediates C and Ce oxidation*

Soft X-ray absorption spectroscopy at the Ce $M_{4,5}$-edges probes electronic transitions between core 3d electrons and valence 4f states, and hence is extremely sensitive to Ce valence and local bonding environment. Fig. 4a shows Ce 3d NEXAFS spectra for $CePO_4{\cdot}H_2O$ samples before and after reaction with catechol under oxic conditions, and a spectrum from $CeO_2$ reference powder. It is evident that the mineral surface has been extensively converted to the oxide during reaction. The data in Fig. 4a were acquired using the surface sensitive total electron yield signal. The simultaneous fluorescence yield signal (not shown) did not give good agreement between weathered $CePO_4{\cdot}H_2O$ and $CeO_2$, indicating that full oxidation was limited to the near surface region only. NEXAFS analysis of control samples showed that the Ce valence was unchanged following reaction with $O_2$ but in the absence of catechol and that no transformation of catechol is observed in the absence of $O_2$ (aq) (Fig. 4b).

NEXAFS spectroscopy at the C K-edge probes molecular bonding via 1s transitions to unoccupied hybridized 2p states (Stöhr, 1992). Carbon NEXAFS is highly sensitive to the presence of unsaturated molecules (double or triple bonds, $\pi^*$ orbitals) and saturated molecules (single bond, $\sigma^*$ orbitals) and different functional groups frequently produce distinct and characteristic peaks that can be used as fingerprints (Stöhr, 1992). Fig. 5 summarizes STXM derived C K-edge NEXAFS spectra of reference organic acids, acquired to assist the characterization of the organic products of reaction, including (a) the spectra of simpler organic acids and (b) the spectra of soil-derived model humic acid compounds and catechol derivatives.

Fig. 6 shows TEY mode C 1s spectra of catechol before and after reaction with $CePO_4{\cdot}H_2O$. The catechol C K-edge spectrum is straightforward to interpret, with strong peaks in the $\pi^*$ region that are attributable to aromatic and phenolic carbon (Cody et al., 1998; Scheinost et al., 2001; Schäfer et al., 2003). The spectral features for catechol after reaction are considerably different, however, indicating the formation of more complex organic molecules. The decrease in the intensity of characteristic catechol peaks is accompanied by the appearance of new $\pi^*$ resonances due to carbon in carboxyl (ca. 288.5 eV) and carbonyl (ca. 289.3 eV) groups, and the development of broad structure in the $\sigma^*$ region characteristic of aliphatic carbon (Myneni, 2003). In summary, the NEXAFS spectroscopic analysis show that, in the presence of catechol, $O_2$ (aq) causes both the oxidation of structural $Ce^{3+}$ and the transformation of catechol to more complex organic molecules.

### 3.3. Catechol transformation with $CeO_2$

STXM measurements on $CeO_2$ samples reacted with catechol are presented in Fig. 7. Spectra characteristic of each species present were extracted and used to derive qualitative component maps using singular value decomposition (SVD) (Koprinarov et al., 2002). SVD is an image sequence fitting procedure that computes a least squares fit of the intensity at each pixel to a linear combination of reference

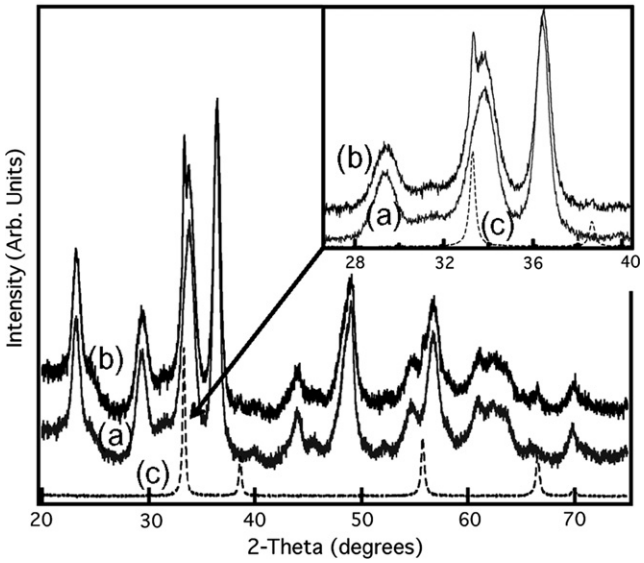


Fig. 3. Powder X-ray diffraction (XRD) analysis of $CePO_4{\cdot}H_2O$ following reaction with catechol and $O_2$. Shown are the patterns of $CePO_4{\cdot}H_2O$ before (a) and after (b) reaction with catechol compared to reference $CeO_2$ (c). The 28–40 degree region of the XRD patterns are enlarged in the inset, showing the presence of a small $CeO_2$ (111) peak in the data from $CePO_4{\cdot}H_2O$ after reaction with catechol.

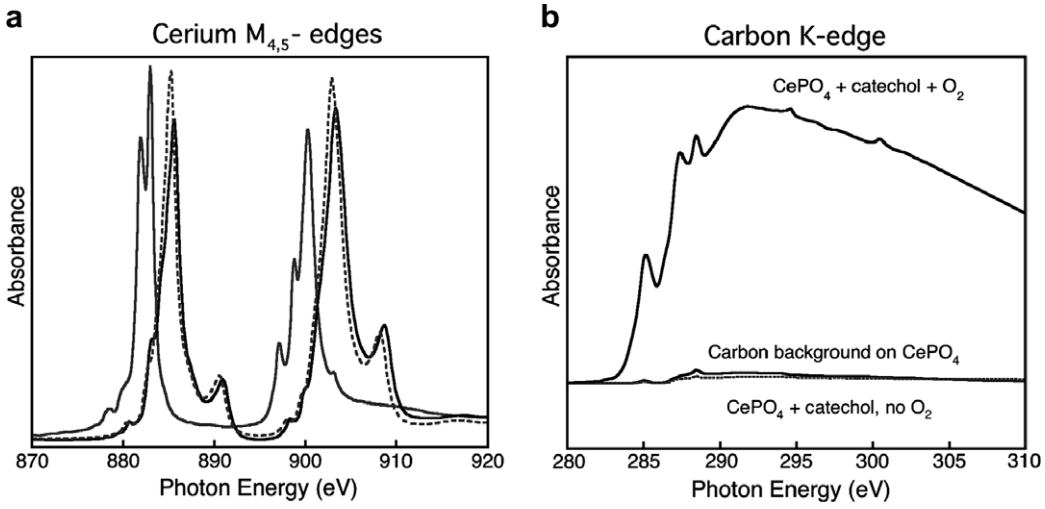


Fig. 4. Near-edge X-ray absorption fine structure (NEXAFS) spectra of the products of the reaction between $CePO_4{\cdot}H_2O$, catechol, and $O_2$. (a) Ce $M_{4,5}$ total electron yield (TEY) spectra of initial (solid black line) and reacted $CePO_4{\cdot}H_2O$ (dashed gray line) compared to reference $CeO_2$ (solid black line). (b) C K-edge NEXAFS spectra of the products of the reaction between $CePO_4{\cdot}H_2O$ and catechol and $O_2$ compared with residual carbon on $CePO_4{\cdot}H_2O$ before reaction in the absence of $O_2$. Spectra were acquired in the total electron yield (TEY) mode. The data show that there is very little carbon contamination on the initial mineral before the addition of catechol. In addition, very little organic material associates with the $CePO_4{\cdot}H_2O$ in the absence of $O_2$.

spectra for each component and was performed using aXis2000 software. Three dominant organic species were found, varying in complexity and association with the inorganic phase. Untransformed catechol is loosely associated with $CeO_2$. On the other hand, more complex organic molecules that exhibit lower aromaticity and stronger C=O $\pi^*$ resonances of carboxyl-C and carbonyl-C groups are only preferentially found in association with the grains. These results show that, in the presence of $O_2$, $CeO_2$ can mediate the oxidative polymerization of catechol to form higher molecular weight polymers.

### 3.4. Catechol transformation with $CePO_4{\cdot}H_2O$

STXM measurements on $CePO_4{\cdot}H_2O$ samples reacted with catechol are presented in Fig. 8. SVD analysis of a stack acquired around the C K-edge reveals that the organic material associated with $CePO_4{\cdot}H_2O$ in the presence of oxygen are typical of the complex molecules produced by $CeO_2$ mediated oxidative polymerization of catechol. Organic material that is not associated with the mineral grains exhibits the lineshape of untransformed catechol. The STXM derived Ce NEXAFS spectra from the mineral did

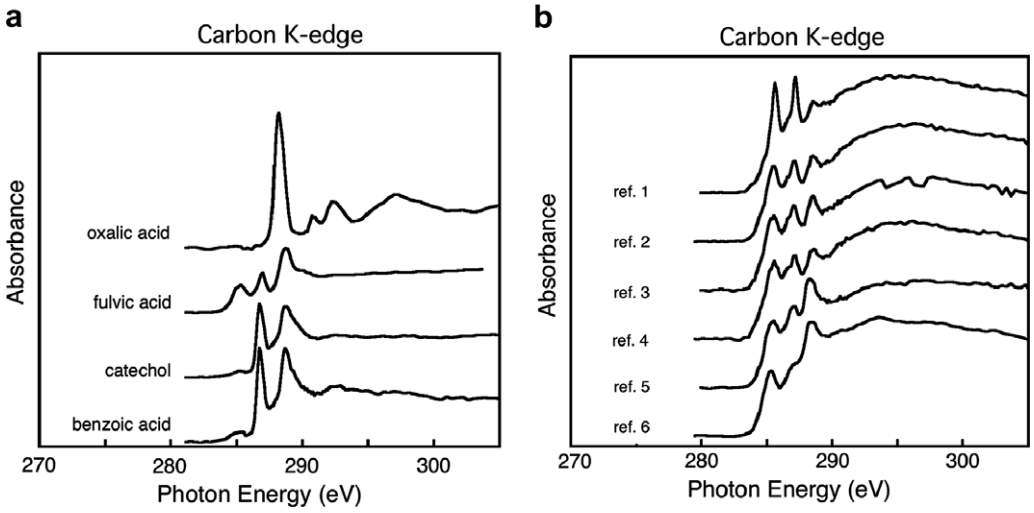


Fig. 5. STXM derived C K-edge NEXAFS spectra of reference organic acids, acquired to assist in the characterization of the organic reaction products. (a) The spectra of simpler organic acids exhibit relatively few absorption peaks that can be directly related to bonds within the molecule. (b) The spectra of soil-derived model humic acid compounds and catechol derivatives are composed of many individual components. Reference compounds 1, 2, and 3, peroxidase extracted humic acid; reference compound 4, 4,5-dichlorocatechol; reference compound 5, 2,3,4-trihydroxybenzoic acid; and reference compound 6, Greenfield humic acid. As described in the main text, the C K-edge analysis show that, out of all the reference organics studied, the catechol-derived natural humic acid materials are chemically most similar to the product of the reaction between catechol, $CePO_4{\cdot}H_2O$, and $O_2$.

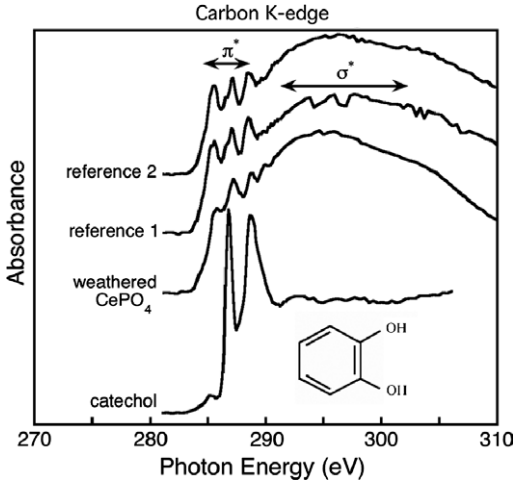


Fig. 6. STXM derived C-K edge NEXAFS spectra of catechol, the organic products of weathering in the presence of $CePO_4{\cdot}H_2O$, and two reference humic substances. Reference 1, "peroxide polymer 3"; reference 2, the peroxide extracted humic acid "catechol 772". Spectra were acquired in transmission mode.

not reveal any presence of Ce(IV). Those spectra were acquired in transmission mode, a bulk sensitive geometry. When compared with surface sensitive TEY spectra, these data indicate that $CeO_2$ formation and subsequent catechol polymerization occurs mostly at the surface of $CePO_4{\cdot}H_2O$ grains.

### 3.5. Organic reaction products

Our results show that the dissolution of $CePO_4{\cdot}H_2O$ by catechol under oxic conditions at pH 5 leads to the formation of dark colored refractory material. This is true after a few days and near-complete coating of mineral particles after 10 days. By comparison, dark coloration did not appear in a stirred control catechol solution at pH 5 exposed to air until at least 500 h after preparation. In other words, direct inorganic reaction of catechol with dissolved oxygen cannot account for by coloration in the $CePO_4{\cdot}H_2O$ dissolution experiments due to variation in C speciation. The dark material was found after reacting $CePO_4{\cdot}H_2O$ and catechol was found to be similar in structure to humic material as evidenced firstly by infrared spectroscopy (Cervini-Silva et al., 2005), and discussed in the present work. Previous reports show that strongly-sorbed humified products formed following reaction of birnessite with catechol, suggesting that such polymerized materials may be common products of mineral surface oxidation of catechol (Machjer et al., 2000). Standard reduction potential magnitude values for manganese oxides and $CeO_2$ are $\leqslant$1.50 and 1.61 V, respectively (Larson, 1998; Sparks, 2003).

Supernatant solution analyses confirmed the presence *albeit* small of oxalate and malate. Our results contrast with a previous report on the quantitative conversion of catechol to malate and oxalate after reaction with commercial $CeO_2$ at 170 °C (Duprez et al., 1996). Data discussed herein shows that surface-formed, small-sized $CeO_2$ following $CePO_4{\cdot}H_2O$ reaction induce the polymerization of organic C. Organically-coated $CeO_2$ nanoparticles have a modified surface structure (Wu et al., 2000) and can exhibit quantum size effects (Yin et al., 2002), which appear to influence mineral reactivity.

Early work (McBride, 1989a) on the transformation of catechol in the presence of birnessite at pH 5.4 reported that oxygen is not consumed during reaction. Those results were explained because Mn(IV) served as the primary

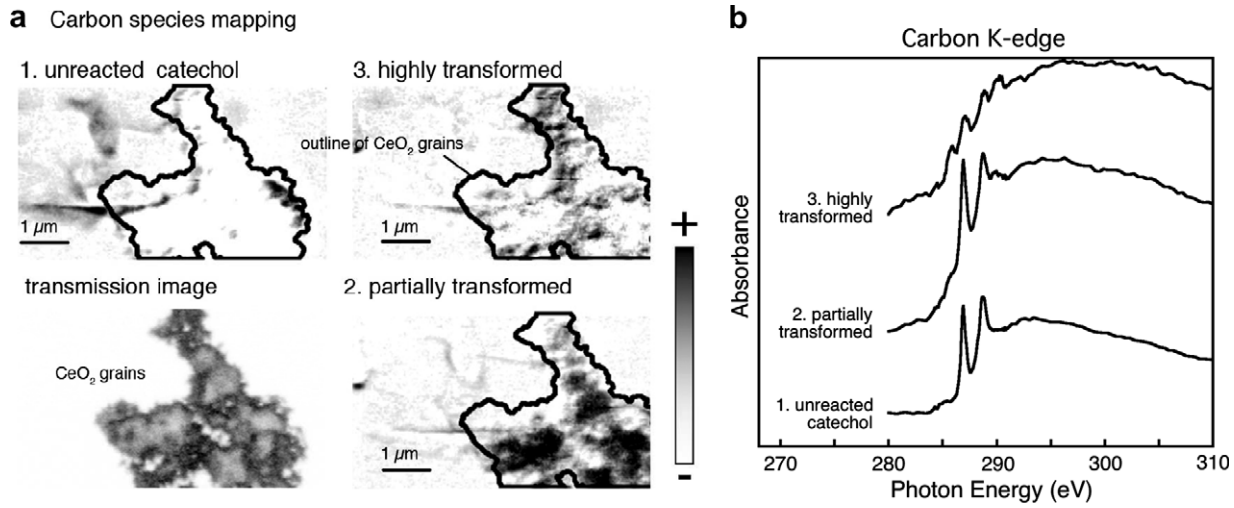


Fig. 7. STXM analysis of the reaction of catechol with $CeO_2$ grains in the presence of $O_2$. Three main organic species were found. (a) The distribution maps of carbon species relative to the $CeO_2$ grains (outline of grains are shown as a solid black line), obtained using singular value decomposition (SVD). (b) The C K-edge NEXAFS spectra of the three dominant species, used in the SVD analysis. The data show catechol which is physically associated with $CeO_2$, can undergo polymerization that is similar or identical to the transformation in the presence of $CePO_4{\cdot}H_2O$.

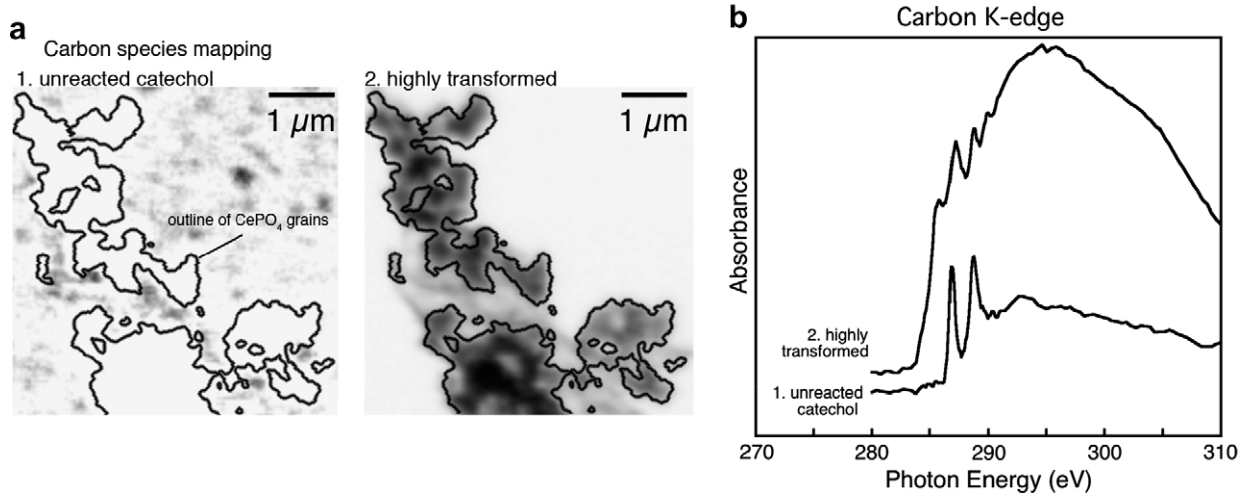


Fig. 8. STXM analysis of the reaction of catechol with $CePO_4{\cdot}H_2O$ grains in the presence of $O_2$, showing that catechol is chemically transformed by the weathering process. (a) Distribution maps of organic species relative to the mineral grains. The outline of the grains (shown as solid black lines) were derived from STXM mapping of the Ce distribution, also shown. The organic species distribution maps were obtained by singular value decomposition (SVD) analysis of the C-K stack. (b) The C K-edge spectra of the two dominant organic species.

oxidant. Along these lines, given the reduction potential values for catechol and Ce(IV) and $O_2$, $E_{Ce(IV)/Ce(III)} = 1.61$ V, $E_{O_2(singlet)/{}^{\bullet}O_2^-} = 0.83$ V, and $E_{catechol\text{–}O^{\bullet}/catechol} = 0.53$ V (Sofen et al., 1979), it is then plausible that Ce(IV) could also serve as primary electron acceptor towards catechol.

We monitored the dissolved oxygen concentration during the reaction between $CePO_4{\cdot}H_2O$ and catechol at $pH_0 = 5$ under oxic conditions. At $t = 0$, dissolved oxygen and catechol initial concentrations were $0.25 \pm 0.1$ and $1 \pm 0.003$ mM, respectively. After 300 h reaction time, the dissolved oxygen concentration was found to remain invariant. These results imply that the activation energy barrier for the oxidation of catechol by molecular oxygen, a diradical species, under prevailing reaction conditions (4:1, oxygen:catechol molar ratio and at room temperature), becomes limiting.

It is worth noting that a significantly higher conversion of catechol under oxic conditions in the presence of nanocrystalline $CeO_2$ formed on $CePO_4.H_2O$ (The solid concentration was 1 g $L^{-1}$ ($c$) and the specific surface area ($S_a$) as determined by the BET method was $66 \pm 1$ $m^2$ $g^{-1}$) than in the presence of commercial $CeO_2$ ($c = 1$ g $L^{-1}$ and $S_a = 19.7 \pm 1$ $m^2$ $g^{-1}$). The reaction of catechol with $CePO_4{\cdot}H_2O$ for 200 h led to the formation of $CO_2$ (73–85% wt C), polymeric C (8–10% wt C), and malate, oxalate, soluble catechol, and sorbed non-polymeric catechol (2–3% wt C). In contrast, the reaction between catechol and $CeO_2$

under similar reaction conditions led to portioning of catechol, namely sorbed, non-polymeric (⩽15% wt C) and dissolved catechol (85% wt C <), with no apparent signature of catechol transformation following the mechanisms mentioned above. These results strongly suggest that (i) Ce(IV) serves as ultimate electron acceptor and (ii) Ce-surface redox properties depend on particle size.

### 3.6. Proposed mechanism for catechol degradation by Ce(IV)

A plausible degradation pathway for catechol by $CePO_4{\cdot}H_2O$ under oxic conditions consistent with our observations involves coupled redox transformations of carbon and cerium at the mineral surface (Figs. 4–8). Oxidation of $Ce^{3+}$ could involve formation of ternary complexes of $Ce^{3+}$ ions, $O_2$, and catechol, analogous to previously described catechol–oxygen–$Mn^{3+}$ complexes (Morrison and Sawyer, 1977; Magers et al., 1978; Pierpont and Buchanan, 1981; Baes and Bloom, 1989; Sheriff, 1992; Gelasco et al., 1998). Complex formation results in a dramatic decrease in redox potential of $Ce^{3+}$, as indicated by the potential values for Ce before and after complexation by catechol, where $E_{Ce(IV)/Ce(III)} = +1.61$ V and $E_{f[Ce(cat)^4]^{4-}/[Ce(cat)^4]^{5-}} = -0.448$ V (Sofen et al., 1979). Thus, the complexed $Ce^{3+}$ can be rapidly oxidized by $O_2$.

The production of $CO_2$, oxalate, malate, and more complex forms of organic carbon following the reaction between $CePO_4{\cdot}H_2O$ and catechol indicates that catechol undergoes oxidation and oxidative polymerization because aromatic-ring rupture (Stevenson, 1994). Charge is transferred from catechol to Ce(IV) ions, leading to semiquinone-based radicals (Stevenson, 1994) that polymerize. Finally, the oxidation of $Ce^{3+}$ to $CeO_2$ is accompanied by an increase in the rate of dissolution of $CePO_4{\cdot}H_2O$ as determined by the rate of accumulation of phosphate in solution (Fig. 1).

## 4. CONCLUSIONS

Here we report a previously unrecognized pathway of cerium biogeochemical cycling that can impact both phosphate and organic carbon cycles in terrestrial ecosystems. It is well known that phosphorous availability is impacted by changes in the redox status of soils and sediments. For instance, under reducing conditions typical of flooded rice fields or in lake sediments, minerals such as strengite [$FePO_4{\cdot}2H_2O$], amorphous ferric phosphate [$FePO_4$], and trivalent manganese phosphate [$MnPO_4{\cdot}1.5H_2O$], undergo reductive dissolution, with the release of P as a consequence (Bingham and Garber, 1960; Bingham, 1963; Moore et al., 1998; Moore, 1999; Moore and Reddy, 1999; Uusitalo and Turtola, 2003). Our results show that cerium redox transformations influence phosphorous bioavailability. In the case of $CePO_4{\cdot}H_2O$, phosphate ions are liberated into solution by cerium oxidation and the sequestration of $Ce^{4+}$ in an insoluble phase ($CeO_2$).

In this paper, we have studied the reaction between $CePO_4{\cdot}H_2O$ and catechol at $pH_0 = 5$ using Scanning Transmission X-Ray Microscopy. Measurements at the C K and Ce $M_{4,5}$ edges that indicate three dominant organic species, varying in complexity and association with the inorganic phase. Untransformed catechol is loosely associated with $CeO_2$, whereas more complex organic molecules that exhibit lower aromaticity and stronger C=O $\pi^*$ resonances of carboxyl-C and carbonyl-C groups are only found in association with the grains. These results further serve as the basis to postulate that, in the presence of $O_2$, $CeO_2$ can mediate the oxidative polymerization of catechol to form higher molecular weight polymers. Also, in this paper we provide NEXAFS spectroscopic analysis to show that, in the presence of catechol, $O_2$ (aq) causes both the oxidation of structural $Ce^{3+}$ and the transformation of catechol to more complex organic molecules.

The higher conversion of catechol under oxic conditions in the presence of nanocrystalline $CeO_2$ formed on $CePO_4{\cdot}H_2O$ compared to commercial $CeO_2$ strongly suggest Ce(IV) serves as ultimate electron acceptor and that surface redox properties depend on particle size. Likely, energetic considerations intrinsic of changes cerium-surface redox properties such as conduction band shiftings following structural Ce oxidation, i.e., mineral transformation, affect kinetics and thermodynamics of intermolecular interactions between carbon species, mineral phases, and confined and bulk water.

In seawater, oxidation of $Ce^{3+}{}_{(aq)}$ by $O_2$ is mediated by microorganisms (Moffett, 1990, 1993). Thus, it has been proposed that $Ce^{3+}{}_{(aq)}$ requires microbial mediation. Data presented herein show that an alternative pathway for $Ce^{3+}{}_{(aq)}$ oxidation is feasible. Our results presented herein are explained because a pathway of biologically-induced, non-enzymatic oxidation of cerium and formation of small $CeO_2$ particles at room temperature. Considerations of the outcome of this work will serve as a basis for the development of a conceptual model for the use of laboratory based experimental studies with sources of organic carbon to interpret the biological fractionation of Ce in paleosols.

Our findings may be also relevant to assessment of the environmental effects of cerium compounds used in technology. $CeO_2$ is manufactured for a wide range of applications, including gas sensors, pigments, and as catalysts for redox reactions in automotive exhaust (Trovarelli, 1996). Nanoparticulate $CeO_2$ has been tested recently as a fuel additive to catalyze combustion reactions between diesel and air (Trovarelli, 1996). Catalyst cartridges bearing commercial $CeO_2$ have been shown to efficiently reduce the concentration of $NO_x$, unburned hydrocarbons, and CO in car exhausts under real running engine conditions (Chung et al., 2003). These applications may lead to the introduction of fine grained, reactive $CeO_2$ into the environment, where it is capable of the low-temperature decarboxylization and polymerization of organic compounds. Consequently, our results highlight the need to study the biogeochemical and toxicological consequences of the release of $CeO_2$ nanoparticles into the environment.


## ACKNOWLEDGMENTS

The authors are most grateful to G. Sposito for providing the natural humic samples; to Andy Yang (University of California) and Pilar Fernández Lomelín (Instituto de Geografía, Universidad

Nacional Autónoma de México) for providing technical support; to J. Coates, M. Finnegan, F. Ogletree, J. Pollock, G. Sposito, T Teague, and G. Vrdoljak for useful comments and access to equipment. S.F. thanks D.K. Shuh, T. Tyliszczak, and M.K. Gilles at BL11.0.2 for providing beamtime. The authors are thankful to Professor David Burdige (Old Dominion University) for providing comments to help improving the manuscript. This research was supported in part by the NASA Astrobiology Institute (1-24190-31020-44) and the Director, Office of Science, of the U.S. Department of Energy under Contract No. DE-AC02-05CH11231. The Advanced Light Source and work at BL11.0.2 STXM and BL 4.0.2 is supported by the Office of Basic Energy Sciences, Division of Materials Sciences, Division of Chemical Sciences, Geosciences, and Biosciences of the DOE at Lawrence Berkeley National Laboratory under contract DOE-AC03-76SF00098.

## REFERENCES

Baes A. U. and Bloom P. R. (1989) Diffuse reflectance and transmission Fourier transformed infrared (DRIFT) spectroscopy of humic and fulvic acids. *Soil Sci. Soc. Am. J.* **53**, 695–700.

Banfield J. F. and Eggleton K. (1989) Apatite replacement and rare earth mobilization, fractionation and fixation during weathering. *Clays Clay Miner.* **37**, 113–127.

Banfield J. F., Barker W. W., Welch S. A. and Tauton A. (1999) Biological impact on mineral dissolution: application of the lichen model to understanding mineral weathering in the rhizosphere. *Proc. Natl. Acad. Sci. USA* **96**, 3404–3411.

Barber D. A. and Martin J. K. (1976) The release of organic substances by cereal roots into soil. *New Phytol.* **76**, 69–80.

Bennett P. C. (1991) Quartz dissolution in organic-rich aqueous systems. *Geochim. Cosmochim. Acta* **55**, 1781–1791.

Bingham F. T. (1963) Relation between P and micronutrients in plants. *Soil Sci. Soc. Am. Proc.* **27**, 389–391.

Bingham F. T. and Garber M. J. (1960) Solubility and availability of micronutrients in relation to phosphorous fertilization. *Soil Sci. Soc. Am. Proc.* **24**, 209–213.

Braun J.-J., Pagel M., Muller J.-P., Bilong P., Michard A. and Guillet B. (1990) Cerium anomalies in lateritic profiles. *Geochim. Cosmochim. Acta* **54**, 781–795.

Brewster J. L., Bhat K. K. S. and Nye P. H. (1976) Possibility of predicting solute uptake and plant-growth response from independently measured soil and plant characteristics. 5. Growth and phosphorous uptake on rape in soil at a range of phosphorous concentrations and a comparison of results with predictions of a simulations-model. *Plant Soil* **44**, 295–328.

Cervini-Silva J., Fowle D. and Banfield J. (2005) Biogenic dissolution of a soil cerium-phosphate mineral. *Amer. J. Sci.* **305**, 711–726.

Chung C. A. H., Livermore S. J. A. and Ormerod R. M. (2003) Internal reforming in intermediate temperature solid oxide fuel cells running on natural gas. *Ionics* **9**, 342–347.

Cody G. D., Ade H., Wirick S., Mitchell G. D. and Davis A. (1998) Determination of chemical–structural changes in vitrinite accompanying luminescence alteration using C-NEXAFS analysis. *Org. Geochem.* **28**, 441–455.

Crews T. E., Kitayama K., Fownes J. H., Riley R. H., Herbert D. A., Mueller-Dombois D. and Vitousek P. O. M. (1995) Changes in soil-phosphorous fractions and ecosystem dynamics across a long cronosequence in Hawaii. *Ecology* **76**, 1407–1424.

Duprez D., Delanoë F., Barbier, Jr., J., Isnard P. and Blanchard G. (1996) Catalytic oxidation of organic compounds in aqueous media. *Catal. Today* **29**, 317–322.

Firsching F. H. and Brune S. N. J. (1991) Solubility products of the trivalent rare-earth phosphates. *J. Chem. Eng. Data* **36**, 93–95.

Gardner W. K., Barber D. A. and Parperry D. G. (1983) The acquisition of phosphorous by *Lupinus albus* L. 3. The probable mechanism by which phosphorous movement in the soil root interface is enhanced. *Plant Soil* **70**, 107–124.

Gelasco A., Bensiek S. and Pecoraro V. L. (1998) The $[Mn_2(2\text{-}OHsalpn)_2]^{2-,1-,0}$ system: an efficient functional model for the reactivity and inactivation of the manganese catalases. *Inorg. Chem.* **37**, 3301–3309.

Green E. G., Macalady J. L. and Banfield J. F. (2002) Biogeochemical contributions to soil formation and landscape lowering. *Eos Trans. AGU*, **83(47)**, # H12B-0929 (abstr.).

Hikichi Y., Hukuo K.-I. and Shiokawa J. (1978) Synthesis of rare earth orthophosphates. *J. Bull. Chem. Soc. Jpn.* **51**, 3645–3646.

Jauregui J. M. S. and Reisenauer H. M. (1982) Calcium-carbonate and manganese dioxide as regulators of available manganese and iron. *Soil Sci.* **134**, 105–110.

Jonasson R. G., Bancroft G. M. and Nesbitt H. W. (1985) Solubilities of some REE phosphates with implications for diagenesis and seawater concentrations. *Geochim. Cosmochim. Acta* **49**, 2133–2139.

Kinrade S. D., Del Nin J. W., Schach A. S., Sloan T. A., Wilson K. L. and Knight T. G. (1999) Stable five- and six-coordinated silicate anions in aqueous solution. *Science* **285**, 1542–1545.

Kirz J., Jacobsen C. and Howells M. (1995) Soft X-ray microscopes and their biological applications. *Q. Rev. Biophys.* **28**, 33–130.

Koprinarov I. N., Hitchcock A. P., McCrory C. T. and Childs R. F. (2002) Quantitative mapping of structured polymeric systems using singular value decomposition analysis of soft X-ray images. *J. Phys. Chem. B.* **106**, 5358–5364.

Kucey R. M. N., Janzen H. H. and Leggett M. E. (1989) Microbially mediated increases in plant-available phosphorous. *Adv. Agron.* **42**, 199–228.

Larson R. A. (1998) *Natural Occurring Antioxidants*. CRC Lewis, Boca Raton.

Larson R. A. and Hufnal, Jr., J. M. (1980) Oxidative polymerization of dissolved phenols by soluble and insoluble inorganic species. *Limnol. Oceanogr.* **25**, 505–512.

Lehmann R. G., Cheng H. H. and Harsh J. B. (1987) Oxidation of phenolic acids by soil iron and manganese oxides. *Soil Sci. Soc. Amer. J.* **51**, 352–356.

Machjer E. H., Chorover J., Bollag J.-M. and Huang P. M. (2000) Evolution of $CO_2$ during birnessite-induced oxidation of $^{14}C$-labeled catechol. *Soil Sci. Soc. Am. J.* **64**, 157–163.

Magers K. D., Smith C. G. and Sawyer D. T. (1978) Polarographic and spectroscopic studies of the manganese(II), -(III), and -(IV) complexes formed by polyhydroxy ligands. *Inorg. Chem.* **17**, 515–523.

McBride M. B. (1989a) Oxidation of 1,2- and 1,4-dihydroxybenzene by birnessite in acidic aqueous suspension. *Clays Clay Miner.* **37**, 479–486.

McBride M. B. (1989b) Oxidation of dihydroxybenzenes in aerated suspensions of birnessite. *Clays Clay Miner.* **37**, 341–347.

Moffett J. W. (1990) Microbially mediated cerium oxidation in sea water. *Nature* **345**, 421–423.

Moffett J. W. (1993) A radiotracer study of cerium and manganese uptake on to suspended particles in Chesapeake Bay. *Geochim. Cosmochim. Acta* **58**, 695–703.

Moore P. A. (1999) Effect of redox potential on phosphorous chemistry in soils and sediments. In Sixth Symposium on Biogeochemistry of Wetlands, Fort Lauderdale, Florida, July 11–14, p. 130.

Moore P. A., Reddy K. R. and Fisher M. M. (1998) Phosphorous flux between sediment and overlying water in lake Okeechobee,

Florida: spatial and temporal variations. *J. Environ. Qual.* **27**, 1428–1439.

Moore P. A. and Reddy K. R. (1999) Role of Eh and pH on phosphorous geochemistry in sediments of lake Okeechobee, Florida. *J. Environ. Qual.* **23**, 955–964.

Morrison M. M. and Sawyer D. T. (1977) Redox reactions of di-μ-oxo bridged binuclear manganese(IV) and -(III) complexes. *J. Am. Chem. Soc.* **99**, 257–258.

Myneni S. C. B. (2003) Soft X-ray spectroscopy and spectromicroscopy studies of organic molecules in the environment. In *Applications of Synchrotron Radiation in Low-Temperature Geochemistry and Environmental Science*, vol. 49 (eds. P. Fenter, M. Rivers, N. Sturchio and S. Sutton), pp. 485–579. Reviews in Mineralogy and Geochemistry. The Mineralogical Society of America, Washington.

Nye P. H. (1977) Rate-limiting step in plant nutrient absorption from soil. *Soil Sci.* **123**, 292–297.

Pierpont C. R. and Buchanan R. M. (1981) Transition metal complexes of *o*-benzoquinone, *o*-semiquinone, and catecholate ligands. *Coord. Chem. Rev.* **38**, 45–87.

Schäfer T., Hertkorn N., Artinger R., Claret F. and Bauer A. (2003) Functional group analysis of natural organic colloids and clay association kinetics using C(1s) spectromicroscopy. *J. Phys. France* **104**, 409–412.

Scheinost A. C., Kretzschmar R., Christl I. and Jacobsen C. (2001). In *Humic Substances: Structures, Models and Functions* (eds. E. A. Ghabbour and G. Davies). Royal Society of Chemistry, Cambridge, pp. 37–40.

Sheriff T. S. (1992) Production of hydrogen-peroxide from dioxygen and hydroxylamine or hydrazine catalyzed by manganese complexes. *J. Chem. Soc. Dalton Trans.* **6**, 1051–1058.

Sofen S. R., Cooper S. R. and Raymond K. N. (1979) Crystal and molecular structures of tetrakis(catecholato)hafnate(IV) and -cerate(IV). Further evidence for a ligand field effect in the structure of tetrakis(catecholate)uranate(IV). *Inorg. Chem.* **18**, 1611–1616.

Sparks D. L. (2003) *Environmental Soil Chemistry*. Academic Press, San Diego.

Stevenson F. J. (1994) *Humus Chemistry: Genesis, Composition, Reactions*. Wiley, New York, pp. 307–317.

Stöhr J. (1992) *NEXAFS Spectroscopy*. Springer-Verlag, Berlin, 392 pp.

Stone A. T. (1987) Reduction and dissolution of manganese(III)/(IV) oxide by substituted phenols. *Environ. Sci. Technol.* **21**, 979–988.

Stone A. T. and Morgan J. J. (1984) Reduction and dissolution of manganese(III) and manganese(IV) oxides by organics. Survey of the reactivity of organics. *Environ. Sci. Technol.* **18**, 617–624.

Stone A. T. and Morgan J. J. (1987) Reduction and dissolution of manganese(III) and manganese(IV) oxides by organics. I. Reaction with hydroquinone. *Environ. Sci. Technol.* **21**, 979–988.

Taunton A. E., Welch S. A. and Banfield J. F. (2000a) Microbial controls on phosphate and lanthanide distributions during granite weathering and soil formation. *Chem. Geol.* **169**, 371–382.

Taunton A. E., Welch S. A. and Banfield J. F. (2000b) Geomicrobiological controls on light rare earth element, Y and Ba distribution during granite weathering and soil formation. *J. Alloys Comp.* **303–304**, 30–36.

Traina S. J. and Doner H. E. (1985) Copper-manganese(II) exchange on a chemically reduced birnessite. *Soil Sci. Soc. Am. J.* **49**, 307–313.

Trovarelli A. (1996) Catalytic properties of ceria and $CeO_2$-containing materials. *Catal. Rev. Sci. Eng.* **38**, 439–520.

Tyliszczak T., Warwick T., Kilcoyne A. L. D., Fakra S., Shuh D. K., Yoon T. H., Brown G. E., Andrews S., Chembrolu V., Strachan J. and Acremann Y. (2004) Soft X-ray Scanning Transmission Microscope working in an extended energy range at the advanced light source SRI 2003. *AIP Conf. Proc.* **705**, 1356–1359.

Ushakov S. V., Helean K. B., Navtrosky A. and Boatner L. A. (2001) Thermochemistry of rare-earth orthophosphates. *J. Mater. Res.* **16**, 2623–2633.

Uusitalo R. and Turtola E. (2003) Determination of redox-sensitive phosphorous in field runoff without sediment preconcentration. *J. Environ. Qual.* **32**, 70–77.

Wang Y. and van Capellen P. A. (1996) Multicomponent reactive transport model of early diagenesis: application to redox cycling in coastal marine environments. *Geochim. Cosmochim. Acta* **60**, 2993–3014.

Welch S. A., Taunton A. E. and Banfield J. F. (2002) Effect of microorganisms and microbial metabolites on apatite dissolution. *Geomicrobiol. J.* **19**, 343–367.

Welch S. A. and Ullman W. J. (1992) The effect of organic acids on plagioclase dissolution rates and stoichiometry. *Geochim. Cosmochim. Acta* **57**, 2725–2736.

Welch S. A. and Vandevivere P. (1994) Effect of microbial and other naturally-occurring polymers on mineral dissolution. *Geomicrobiol. J.* **12**, 227–238.

Welch S. A., Barker W. W. and Banfield J. F. (1999) Microbial extracellular polysaccharides and plagioclase dissolution. *Geochim. Cosmochim. Acta* **63**, 1405–1419.

Wu Z., Guo L., Li H., Yang Q. and Zhu H. (2000) EXAFS study on the local atomic structures around Ce in $CeO_2$ nanoparticles. *Mater. Sci. Eng. A* **286**, 179–182.

Yin L., Wang Y., Pang G., Koltypin Y. and Gedanken A. (2002) Sonochemical synthesis of cerium oxide nanoparticles—effect of additives and quantum size effect. *J. Colloid Interface Sci.* **246**, 78–84.

Young A. T., Feng J., Arenholz E., Padmore H. A., Henderson T., Marks S., Hoyer E., Schlueter R., Kortright J. B., Martynov V., Steier C. and Portmann G. (2001) First commissioning results for the elliptically polarizing undulator beamline at the advanced light source. *Nucl. Instrum. Meth. Phys. Res. A* **467–468**, 549–552.